Development of a Transmission-Based Open-Ended Coaxial-Probe Suitable for Axillary Lymph Node Dielectric Measurements

Matteo Savazzi[1], Emily Porter[2, 3], Martin O'Halloran[3], Jorge R. Costa[4], Carlos Fernandes[4], João M. Felicío[4], Raquel C. Conceição[1]

[1] Instituto de Biofísica e Engenharia Biomédica, Faculdade de Ciências, Universidade de Lisboa, 1749-016 - Lisbon, Portugal, mlsavazzi@fc.ul.pt, rcconceicao@fc.ul.pt

[2] Department of Electrical and Computer Engineering, The University of Texas at Austin, Austin, TX, USA

[3] Translational Medical Device Lab, National University of Ireland Galway, University Road, Galway, Ireland

[4] Instituto de Telecomunicações IST, Universidade de Lisboa, Lisbon, Portugal, joao.felicio@lx.it.pt

***Abstract* —** We assess the feasibility of a transmission-based open-ended coaxial-probe for tissue dielectric properties estimation. The ultimate goal is to use it for axillary lymph node dielectric measurement, which is not trivial when applying the state-of-the-art reflection-based open-ended coaxial-probe. The proposed technique consists in placing the material under test between two opposite open-ended coaxial-probes and record the transmission coefficient. We numerically assess three coaxial probe configurations, in order to ensure adequate transmission and sensing volume. The final setup allows for enough propagation through a 5*mm* sample (which will be sufficient for the measurements of axillary lymph nodes), while confining the sensing volume to the region of interest. Experimental tests on two materials of different permittivity ranges showed good agreement between the measured and numerical transmission coefficient. Moreover, we observed that the transmission coefficient can highlight the contrast between materials with different dielectric properties. The promising initial results motivate the further application of the method to the case of axillary lymph nodes.

***Index Terms* — breast cancer, coaxial-probe, complex permittivity measurement, microwaves, transmission coefficient, sensing volume.**

I. Introduction

Breast cancer is the most frequently diagnosed and cause of cancer death among women [1]. The cancer spread beyond the breast (termed metastasis) is the leading cause of death in breast cancer patients. Axillary Lymph Nodes (ALNs) drains 75% of the lymph from the breast and they are often the first location to which breast cancer metastasis spread. For this reason, ALN diagnosis is clinically vital in breast cancer and the disease status of these nodes is a significant prognostic factor for guiding treatment selection [2]. Currently, Sentinel lymph Node Biopsy (SNB) is the state-of-the-art method for ALN diagnosis. SNB relies on findings [3, 4], which showed that breast cancer firstly spread to one or a few ALNs, known as the sentinel ALN, before it spreads to other ALNs [3, 4]. The sentinel ALN can be identified using vital blue dye and/or radio-labeled colloid [3, 4]. Following these findings, the practice of ALN identification and excision (i.e. SNB) has become widely adopted in developed countries. However, the sensitivity of the method strongly relies on the physician's experience and intuition [2]. Therefore, high risk of pre-emptive ALN removal is associated with SNB. This can lead to long patient's recovery, risk of infection and lymphedema [5, 6]. Despite the widespread adoption of SNB, having prior information about modifications in the ALN is highly valuable, which justifies the need for imaging methods to detect and analyze the ALNs non-invasively.

MicroWave Imaging (MWI) is a promising imaging technique, which is being proposed for several applications, including breast cancer diagnosis [7-9]. This technique relies on the contrast of dielectric properties between healthy and malignant tissue at microwave (MW) frequencies (typically in the range of 1-10 GHz). MWI presents several advantages compared to other imaging systems, namely the fact it is potentially low-cost, it uses non-ionizing radiation, it is non-invasive, and the device can be portable. Despite the vast literature on MWI, only a few studies addressed the possibility of imaging ALN with this technique [10, 11]. In order to validate MWI as a potential tool for ALN screening, it is crucial to quantify the contrast between healthy and metastasized ALNs. However, the measurement of ALN dielectric properties is not trivial, due to the heterogeneity of the tissue, which is a critical issue in the application of the state-of-the-art method (i.e. the Open-Ended Coaxial-Probe).

Several methods have been proposed for biological tissue dielectric measurement, such as transmission line, resonant cavity, multielectrode probe, and Reflection-based Open-Ended Coaxial-Probe (R_xOECP). Among these methods, the R_xOECP is the most commonly used and provides ground truth for several studies [12, 13]. Such widespread adoption is due to diverse reasons: tissue handling is minimal and non-destructive; and both *ex vivo* and *in vivo* measurement over a broad frequency range are possible [12, 14]. However, the interpretation of the R_xOECP measurement is not trivial when involving heterogeneous tissues [15]. The penetration

depth of the sensing volume is generally on the order of fractions of a millimeter [16], which is critical when the outer layer of the sample differs from the inner tissue. This is the case of ALNs, which, after their excision, are often surrounded by a variable amount of fat. The fat layer covering the ALN affects the estimated permittivity and tends to confound the measurement. In this context, we would need a more in-depth sensing volume, which is capable of retrieving average information of specimen of an organ that is covered by a "confounding" superficial layer.

Meaney et al. recently developed a Transmission-based Open-Ended Coaxial-Probe method, which is intended for the measurement of vertebrate dielectric properties [17]. In this configuration, two Open-Ended Coaxial-Probes (OECPs) are immersed inside the material under test (MUT) facing each other. The probes work as two "low-efficiency antennas", and the measured transmission coefficient (S_{21}) is used to analytically solve the complex permittivity of the MUT. However, Meaney's method is inapplicable to the case of ALN dielectric measurement, due to different reasons. Firstly, the analytical formulation proposed to de-embed dielectric properties assumes that the electromagnetic (EM) field reflections on the MUT-air interface are negligible. That hypothesis is not realistic in the case of ALN measurement due to the limited size of ALNs (ALN size ranges from 0.5*cm* to 2*cm* along their larger axis). Secondly, the method requires the measurement of the S_{21} at several separation distances, which implies the penetration of the tissue with the probes. This is not feasible in the case of ALN, which cannot be punctured, as demanded by clinicians.

In this paper, we present a Transmission-based Open-Ended Coaxial-Probe (which will be onwards referred to as T_xOECP) which is instead designed for relatively small size (few millimeters) heterogeneous samples. In particular, we aim at developing a probe capable of an elongated sensing volume rather than a transversal field spread. Moreover, given the inapplicability of the analytical formulation proposed in [7], we investigated an alternative approach for the de-embedding of dielectric properties.

The structure of the paper is as follows. Section II describes the preliminary numerical tests used to investigate the feasibility of a T_xOECP, together with a study of the design of the probe which could provide the sensing volume that best suits our requirements. Section III describes the experimental results obtained when measuring phantoms with the developed T_xOECP. Lastly, the conclusions and future work are discussed in Section IV.

II. Numerical Assessment of a T_xOECP

To investigate the feasibility of a T_xOECP, we performed preliminary numerical tests. As a first test, we compared the behavior of three different probe designs. The goal was to maximize the magnitude of the transmission coefficient, S_{21}, through the sample, while focusing the EM-field towards the receiving probe (i.e. along the *z*-axis in Fig.1.a). As represented on the left side of Fig. 1, the three setups consist of two coaxial-probes "sandwiching" a cylindrical sample. The RF energy (emitted by the first probe) propagates through the MUT over a distance *d*, as marked in Fig. 1.a. The three T_xOECP setups differ in the design of their coaxial-probe cut-off sections (i.e. the tips of the OECPs which are in contact with the MUT). In detail, the tested OECPs were the following:

- Probe (a): *Cut flush* OECPs (Fig. 1.a)
- Probe (b): OECPs with *recessed* outer conductor (Fig.1.b). In this configuration, we removed the outer conductor from the last segment (last 2*mm*) of the OECPs. This was done to enhance the transmission ability of the OECP. Indeed, by shortening the outer conductor, we aimed at making the emitting probe slightly radiative.
- Probe (c): OECPs with metal flanges (Fig. 2.1c). By adding flanges, we aimed at creating a cavity to stuck the EM energy out of the cable, while minimizing the electric field (E-field) dispersion outside the sample.

For the three tested configurations, Fig. 2 reports the $|S_{21}|$ of a cylindrical MUT (Fig 1.a). The MUT has radius *r*=5mm,

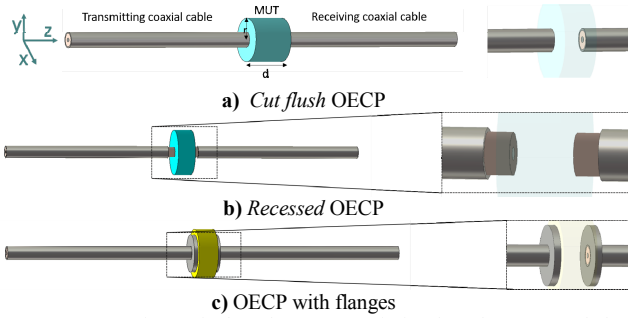

Figure 1: Design of the three transmission-based Open-Ended Coaxial-Probes (TxOECP), tested in simulation: (a) *cut flush* TxOECP; (b) *recessed* TxOECP; (c) TxOECP with flanges. In (a), the tips of the coaxial probes were not modified. In (b), the outer conductor was removed from the tips of the coaxial probes. In (c), two metal flanges were placed at the tips of the coaxial probes. On the right side of the figure, the detailed views of the probe tips are shown.

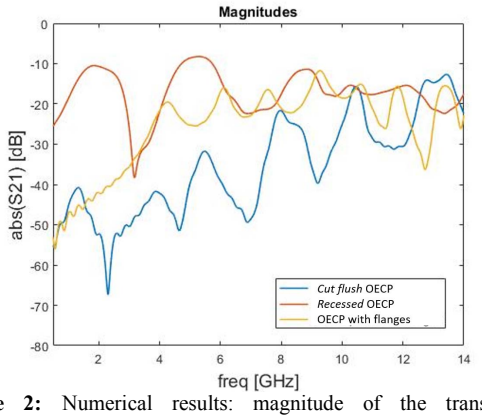

Figure 2: Numerical results: magnitude of the transmission coefficient, S_{21}, for the three probe tip configurations under study (see Fig.1.a). The material under test is a cylindrical sample as shown in Fig. 1.a. Parameter values: radius *r*=5*mm*; separation distance *d*=5*mm*; relative permittivity ε^{l}=55; conductivity σ=1*S/m*.

separation distance d=5mm, relative permittivity ε^{l}=55, and conductivity σ=1S/m.

We observed that both the partial removal of the outer conductor (Fig. 1.b) and the application of flanges (Fig. 1.c) increase the transmission capability of the T_xOECP. This is a positive result since larger magnitude S_{21} may enhance the sensitivity of the method.

We also analysed the E-field inside the MUT, in order to assess how it would spread along the transversal direction over the entire volume of the sample. If the E-field spreads over a very large area along *xy*-plane, the de-embedded permittivity value will be an "average" over the entire volume of the sample. This is highly undesired since ALNs often occupy just a small portion of the excised sample. The E-field magnitude map at 6GHz is reported in Fig. 3 for the three probes. The analysis of this plot leads to the following considerations:

- In Fig. 3.a, the *cut flush* OECPs showed good results in confining the E-field to a small area of the sample;
- In Fig 3.b, the E-field plot suggests that the *recessed* OECPs radiates out of the region of the sample, making this configuration unsuitable for our application;
- In Fig. 3.c, the E-field plot suggests that the addition of the flanges causes a spreading effect of the E-field over the volume of the sample. This behaviour is undesired since the sensing volume of the probe should be limited to a confined region. In particular, the E-field should propagate along the *z*-axis, limiting as much as possible its spatial spreading on the *xy*-plane. It is expected that this effect increases the dependence of the technique on the sample size.

Given the limitations presented by probe configurations (b) and (c), we decided to adopt configuration (a), which presented the best trade-off between transmitted power and sensing volume. Yet, we will most probably have some limitations regarding the *z*-dimension of the samples, since for large values of d the signal to noise ratio may deteriorate significantly.

Finally, we investigated the influence of the radius of the MUT on the magnitude of S_{21}. In other words, we analysed if the $|S_{21}|$ is affected by changes of the transversal dimensions of the MUT. Fig. 4 shows the $|S_{21}|$ for several samples, with different radius (details on the MUT size and dielectric properties are reported in the figure). The results indicate that the $|S_{21}|$ is not stable over changes of the sample size in the *xy*-plane. The size (and probably the shape) of the sample influence the S_{21} and has to be taken into account when de-embedding the dielectric properties of any MUT.

In a nutshell, the *cut flush* T_xOECP can transmit enough power through an ALN ($|S_{21}|$ greater than the VNA dynamic range), while confining the EM-field to a limited region of the sample. Moreover, the size of the sample influences the transmission, which is probably due to the reflections which occur at the air-MUT interface. For these reasons, keeping track of the size (and, if possible, of the shape) of the measured sample will be crucial for the success of the measurements.

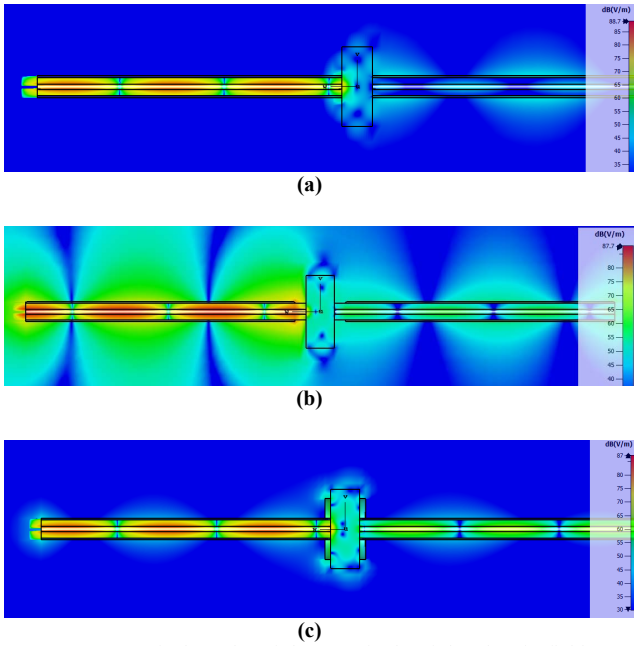

(a) **(b)** **(c)**

Figure 3: Numerical results of the magnitude of the electric field (at 6GHz) for the three probe configurations under study: (a) *cut flush* Coaxial Probe; (b) Coaxial Probe with peeled-off outer conductor; (c) Coaxial Probe with flanges.

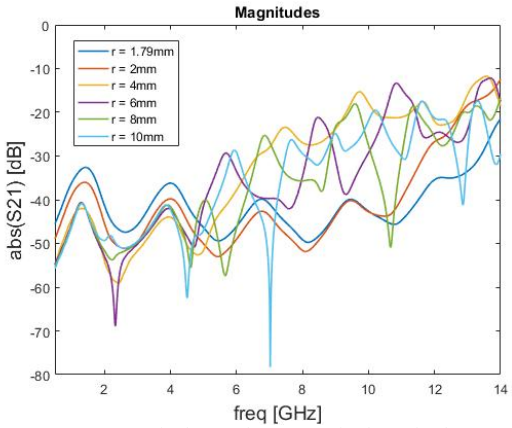

Figure 4: Numerical results: magnitude of the transmission coefficient, $|S_{21}|$, using probe (a). The results of different radius samples are compared. Other parameter values: separation distance d=5*mm*; relative permittivity ε^{l}=55; conductivity σ=1*S/m*.

III. EXPERIMENTAL RESULTS

Following the numerical results described in Section II, we fabricated the setup using the *cut flush* OECPs (configuration (a)). Fig. 5 shows a photograph of the measurement setup, which consists of the following components: one VNA (not included in the photograph) connected to the two (semi-rigid) OECPs (EZ-141 with diameter of 3.58 *mm*); one 3D-printed Polylactic Acid (PLA)

Figure 5: Experimental setup employed for transmission-based dielectric measurements. The two open-ended coaxial-cables are embedded in a plastic support and connected to a 2-port VNA (not shown in the figure). A caliper serves to measure the separation distance between the probes. Between the probes, a phantom is measured.

structure which serves both as (i) holder for the OECPs and (ii) support table for the MUT; one integrated caliper to measure the thickness of the MUT (i.e. the separation distance *d* between the two probes).

The de-embedding of dielectric properties relies on the empirical comparison between experiments and simulations. The method is based on the hypothesis that an accurate representation of the experiments in simulation should give approximately the same output (same S_{21}) of the actual experiments. This approach is inspired by the study published in [18], which showed good agreement between experimental and numerical transmission coefficient when using a similar setup to de-embed the dielectric properties of liquids. We note that although PLA has a relative permitivity of around 2.75 [19], numerical results have shown that the PLA support does not affect the results significantly. Therefore, the numerical setup for the de-embedding of the properties of MUT does not include the entire structure, but rather just the OECPs and MUT.

We performed experimental and numerical measurements on two different phantoms with known dielectric properties and sizes. The measured phantoms were:

- One cuboid sample (25mm x 25mm x 1.77mm) made of acrylic;
- One cuboid phantom (19mm x 19mm x 1.62mm) made of the following mixture: 7.5% w/w graphite; 7% w/w Carbon Black, 85.5% w/w Polyurethane; and 4ml isopropanol per 100*g* of mixture. (This mixture was originally produced for different research purposes, as reported in [20]).

The complex permitivities of the two materials were measured with the R_xOECP and are reported in Fig. 6. Numerical and experimental results are compared in Fig.7, indicating good agreement both for the acrylic (blue plots) and the mixture (red plots) cases. Moreover, a clear separation between the S_{21} of the two materials is observed (note the separation between the blue and red plots in Fig. 7). This result suggests that the transmission coefficient, measured with our T_xOECP, may be able to discriminate between dielectric properties of different materials.

As a final test, we measured (just through simulation) the S_{21} relative to a cuboid sample (19mm x 19mm x 1.62mm), composed of two layers (interface perpendicular to the z-axis), which have respectively the dielectric properties of the acrylic and of the above described mixture. Interestingly the S_{21} falls between those of the two homogeneous materials, suggesting the need to complete further tests to assess the viability of this system to measure average dielectric properties of heterogeneous samples.

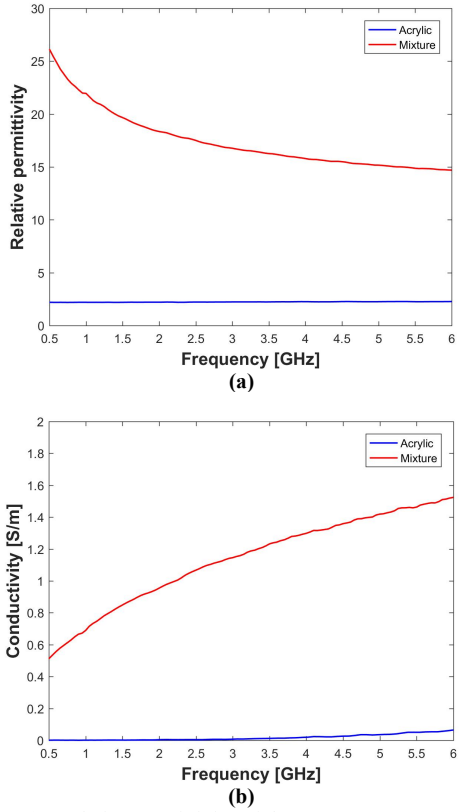

Figure 6: (a) Relative permittivity of the two MUT measured with the TxOECP; (b) Equivalent conductivity. These values were obtained using the RxOECP and serve only as benchmark to assess the sensitivity of the TxOECP technique.

IV. Conclusions and Future Work

We assessed the feasibility of a transmission-based setup using two open-ended coaxial probes for the estimation of dielectric properties of biological tissues. Contrarily to the traditional reflection-based coaxial probe, the proposed setup provides deeper sensing volume while keeping acceptable transmitted power.

We studied the transmission coefficient magnitude and electric field spread over the MUT for three probe configurations. We concluded that the *flush cut* OECPs best fit our requirements on the sensing volume and transmitted power. We fabricated the setup and measured two samples with different relative permittivity values. The experimental results showed acceptable match with numerical results, which is quite promising regarding the feasibility of the technique.

The next step will be the application of the method to the measurement of ALNs, which is the ultimate goal of this research. We expect that we may have to handle issues due to the irregular shape of biological tissues which cannot be

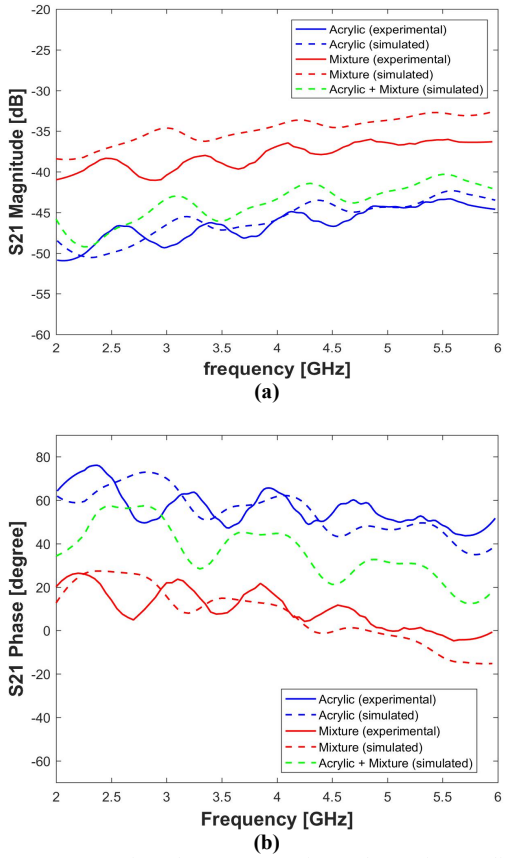

Figure 7: Comparison between experimental (continuous line) and simulated (dashed line) S_{21} obtained when measuring two different permittivity samples. Sample dielectric properties are reported in Fig.6. Propagation distance: d=1.77*mm* (acrylic case); d=1.62*mm* (mixture case): (a) Magnitude of transmission coefficient; (b) Phase of transmission coefficient.

easily reproduced in Computed Aided Design (CAD) environment.

ACKNOWLEDGMENT

This work was supported by the EMERALD project funded from the European Union's Horizon 2020 research and innovation programme under the Marie Skłodowska-Curie grant agreement No. 764479.

This work is also supported by Fundação para a Ciência e a Tecnologia-FCT, FCT/MEC (PIDDAC) under the Strategic Programme UID/BIO/00645/2020.

The author would like to acknowledge Carlos Brito and António Almeida for the support given in the design and fabrication of the setup, as well as in the experimental work.

REFERENCES

[1] International Agency for Research on Cancer - World Health Organization, "GLOBOCAN 2018: Estimated Cancer Incidence, Mortality and Prevalence Worldwide in 2018 - Cancer Fact Sheets," 2018. [Online]. Available: http://gco.iarc.fr/today/fact-sheets-cancers

[2] G. H. Lyman et al., "American Society of Clinical Oncology Guideline Recommendations for Sentinel Lymph Node Biopsy in Early-Stage Breast Cancer", *Journal of Clinical Oncology*, 23(30), pp. 7703-7720, 2005.

[3] U. Veronesi et al., "A Randomized Comparison of Sentinel-Node Biopsy with Routine Axillary Dissection in Breast Cancer", *The New England Journal of Medicine*, 340(6), pp. 546-553, 2003.

[4] D. L. Morton et al., "Validation of the Accuracy of Intraoperative Lymphatic Mapping and Sentinel Lymphadenectomy for Early-Stage Melanoma: a Multicenter Trial", *Annals of Surgery*, 230(4), pp. 453, 1999.

[5] S. G. Komen, "Facts for Life: Axillary Lymph Node," 2009. [Online]. Available: http://ww5.komen.org/uploadedfiles/Content_Binaries/806-392a.pdf

[6] H. Rahbar, S. C. Partridge, S. H. Javid, and C. D. Lehman, "Imaging Axillary Lymph Nodes in Patients with Newly Diagnosed Breast Cancer", *Current Problems in Diagnostic Radiology*, 41(5), pp. 149-158, 2012.

[7] S. C. Hagness, A. Taflove, and J. E. Bridges, "Two Dimensional FDTD Analysis of a Pulsed Microwave Confocal System for Breast Cancer Detection: Fixed-Focus and Antenna-Array Sensors", *IEEE Transactions on Biomedical Engineering*, 45, pp. 1470-1479, 1998.

[8] Y. Xie, B. Guo, L. Xu, J. Li, and P. Stoica, "Multistatic Adaptive Microwave Imaging for Early Breast Cancer Detection", *IEEE Transactions on Biomedical Engineering*, 53(8), pp. 1647-1657, 2006.

[9] R. C. Conceição et al., *An Introduction to Microwave Imaging for Breast Cancer Detection* (Biological and Medical Physics, Biomedical Engineering). Switzerland: Springer, 2016.

[10] R. Eleutério, A. Medina, and R. Conceição, "Initial Study with Microwave Imaging of the Axilla to Aid Breast Cancer Diagnosis," IEEE APS-URSI, Memphis, TN, USA, 2014.

[11] J. Liu and S. G. Hay, "Prospects for Microwave Imaging of the Lymphatic System in the Axillary," IEEE APWC, Cairns, Australia, 2016.

[12] S. Gabriel, R. W. Lau, and C. Gabriel, "The Dielectric Properties of Biological Tissues: II. Measurements in the Frequency Range 10 Hz to 20 GHz", *PHYSICS IN MEDICINE AND BIOLOGY*, 41, pp. 2251-2269, 1996.

[13] M. Lazebnik et al., "A Large-Scale Study of the Ultrawideband Microwave Dielectric Properties of Normal Breast Tissue Obtained from Reduction Surgeries", *PHYSICS IN MEDICINE AND BIOLOGY*, 52, pp. 2637–2656, 2007.

[14] A. Peyman, S. Holden, and C. Gabriel, "Mobile Telecommunications and Health Research Programme: Dielectric properties of tissues at Microwave Frequencies", *Microwave Consultants Limited: London, UK*, pp. 2005.

[15] A. La Gioia, M. O'Halloran, A.Elahi, and E. Porter, "Investigation of Histology Radius for Dielectric Characterisation of Heterogeneous Materials", *IEEE Transactions on Dielectrics and Electrical Insulation*, 25(3), pp. 1064-1069, 2018.

[16] P.M. Meaney, A. Gregory, N. Epstei, and K. D. Paulsen, "Microwave Open-Ended Coaxial Dielectric Probe: Interpretation of the Sensing Volume re-Visited", *BMC Medical Physics*, 14, pp. 2014.

[17] P.M. Meaney, T. Rydholm, and H. Brisby, "A Transmission-Based Dielectric Property Probe for Clinical Applications", *Sensors*, 18(10), pp. 3484, 2018.

[18] A. Kiourti, J. R. Costa, C. A. Fernandes, A. G. Santiago, and K. S. Nikit, "Miniature Implantable Antennas for Biomedical Telemetry: from Simulation to Realization", *IEEE Transactions on Biomedical Engineering*, 59(11), pp. 3140-3147, 2012.

[19] João M Felício, Carlos A Fernandes, and Jorge R Costa, "Complex permittivity and anisotropy measurement of 3D-printed PLA at microwaves and millimeter-waves," Complex permittivity and anisotropy measurement of 3D-printed PLA at microwaves and millimeter-waves. 1-6: IEEE, 2016.

[20] Barry McDermott et al., "Stable tissue-mimicking materials and an anatomically realistic, adjustable head phantom for electrical impedance tomography", *Biomedical Physics & Engineering Express*, pp. 2017.